Photoaging of Phenolic Secondary Organic Aerosol in the Aqueous Phase: Evolution of Chemical and Optical Properties and Effects of Oxidants

Wenqing Jiang[1,2], Christopher Niedek[1,2], Cort Anastasio[2,3], Qi Zhang[1,2*]

5   [1]Department of Environmental Toxicology, University of California, 1 Shields Ave., Davis, CA 95616, USA
[2]Agricultural and Environmental Chemistry Graduate Program, University of California, 1 Shields Ave., Davis, CA 95616, USA
[3]Department of Land, Air, and Water Resources, University of California, 1 Shields Ave., Davis, CA 95616, USA

Correspondence to: Qi Zhang (dkwzhang@ucdavis.edu)

10   **Abstract.** While gas-phase reactions are well established to have significant impacts on the mass concentration, chemical composition, and optical properties of secondary organic aerosol (SOA), the aqueous-phase aging of SOA remains poorly understood. In this study, we performed a series of long-duration photochemical aging experiments to investigate the evolution of the composition and light absorption of the aqueous SOA (aqSOA) from guaiacyl acetone (GA), a semivolatile phenolic carbonyl that is common in biomass burning smoke. The aqSOA was produced from reactions of GA with hydroxyl radical

15   ($\bullet$OH-aqSOA) or a triplet excited state of organic carbon (^{3}C*-aqSOA) and was then photoaged in water under conditions that simulate sunlight exposure in northern California for up to 48 hours. The effects of increasing aqueous-phase $\bullet$OH or ^{3}C* concentration on the photoaging of the aqSOA were also studied. High resolution aerosol mass spectrometry (HR-AMS) and UV-vis spectroscopy were utilized to characterize the composition and the light absorptivity of the aqSOA and to track their changes during aging.

20   Compared to $\bullet$OH-aqSOA, the ^{3}C*-aqSOA is produced more rapidly and shows less oxidation, a greater abundance of oligomers, and higher light absorption. Prolonged photoaging promotes fragmentation and the formation of more volatile and less light-absorbing products. More than half of the initial aqSOA mass is lost and substantial photobleaching occurs after 10.5 hours of prolonged aging under simulated sunlight illumination for ^{3}C*-aqSOA and 48 hours for $\bullet$OH-aqSOA. By performing positive matrix factorization (PMF) analysis of the combined HR-AMS and UV-vis spectral data, we resolved three generations

25   of aqSOA with distinctly different chemical and optical properties. The first-generation aqSOA shows significant oligomer formation and enhanced light absorption at 340-400 nm. The second-generation aqSOA is enriched in functionalized GA species, while the third-generation aqSOA contains more fragmented products and is the least light-absorbing. Although photoaging generally increases the oxidation of aqSOA, a slightly decreased O/C of the $\bullet$OH-aqSOA is observed after 48 hours of prolonged photoaging with additional $\bullet$OH exposure. This is likely due to greater fragmentation and evaporation of highly

30   oxidized compounds. Increased oxidant concentration accelerates the transformation of aqSOA and promotes the decay of brown carbon (BrC) chromophores, leading to faster mass reduction and photobleaching. In addition, compared with $\bullet$OH,

photoaging by ^{3}C* produces more low-volatility functionalized products, which counterbalances part of the aqSOA mass loss due to fragmentation and evaporation.

1. Introduction

35   Phenols, which are emitted from biomass burning (BB) through lignin pyrolysis (Schauer et al., 2001) and formed from the oxidation of aromatic hydrocarbons (Berndt and Böge, 2006), are important precursors for atmospheric secondary organic aerosol (SOA) and brown carbon (BrC) (Bruns et al., 2016; Mabato et al., 2022; Misovich et al., 2021; Smith et al., 2016; Sun et al., 2011; Yee et al., 2013). These compounds can form aqueous-phase SOA (aqSOA) at fast rates in atmospheric waters, through photoreactions with oxidants such as hydroxyl radical (•OH), excited triplet states of organic carbon (^{3}C*), and reactive

40   nitrogen species (e.g., •NO, •NO$_2$, NO$^+$, and NO$_2^+$) (Jiang et al., 2021b; Mabato et al., 2022; Pang et al., 2019; Yang et al., 2021; Yu et al., 2014). The mass yields of phenolic aqSOA range from 50% to 140%, and the proposed formation pathways include oligomerization, hydroxylation, functionalization, demethoxylation, and fragmentation (Arciva et al., 2022; Huang et al., 2018; Jiang et al., 2021a; Ma et al., 2021; Smith et al., 2014, 2015, 2016; Sun et al., 2010; Yu et al., 2014, 2016). Reactions involving reactive nitrogen species can also lead to nitration and nitrophenol formation (Heal et al., 2007; Mabato et al., 2022;

45   Pang et al., 2019; Yang et al., 2021). The resulting phenolic oligomers, multifunctional derivatives, and nitrophenols can absorb near-UV and visible light and contribute significantly to BrC formation in biomass burning emissions (Gilardoni et al., 2016; Li et al., 2022; Misovich et al., 2021; Palm et al., 2020; Pang et al., 2019). In addition, humic-like substances (HULIS), which can induce oxidative stress and cause adverse health effects (Deng et al., 2022), are observed in phenolic aqSOA as well (Chang and Thompson, 2010).

50   Despite extensive research on the formation of aqSOA from phenols, the aging and degradation of phenolic SOA in water remain poorly characterized. Atmospheric lifetimes of SOA range from hours to weeks (Wagstrom and Pandis, 2009), during which chemical reactions can occur, leading to continuous aging and evolution of SOA. Functionalization (i.e., the addition of functional groups to the molecules) and fragmentation (i.e., the breaking of bonds within the molecules to form smaller species) are critical mechanisms in the aging of SOA that can greatly change the chemical composition and loading of aerosols (Kroll

55   et al., 2009; Leresche et al., 2021; Shrivastava et al., 2017). Chemical aging can also influence the optical properties of SOA, as some reactions increase the light absorptivity while others cause photobleaching by destroying chromophores (Lee et al., 2014). Furthermore, fragmentation can result in the formation of volatile and semivolatile products, causing a loss of SOA mass and photobleaching (Kroll et al., 2015). Yu et al. (2016) studied the aqueous-phase photooxidation of phenol and methoxyphenols and observed that, as aging progresses, fragmentation reactions become increasingly dominant in comparison

60   to oligomerization and functionalization reactions. However, a portion of the aqSOA appears to be resistant to fragmentation and remains chemically unchanged even after prolonged exposure to simulated sunlight in the aqueous phase (Yu et al., 2016). Similarly, in an environmental chamber study, O'Brien and Kroll (2019) reported that 70−90% of the α-pinene SOA mass remained in particles after an initial decay during photochemical aging.

The impacts of aging on the concentrations and properties of SOA in the atmosphere have been widely observed in biomass
65   burning emissions (Brege et al., 2018; Chen et al., 2021; Garofalo et al., 2019; Kleinman et al., 2020; Zhou et al., 2017). For
instance, aged wildfire plumes subjected to aqueous processing experience substantial losses in organic aerosol (OA) mass,
increases in SOA oxidation, and changes in optical properties (Che et al., 2022; Farley et al., 2022; Sedlacek et al., 2022).
Aqueous-phase oxidation of organic molecules, including phenols, and the formation of SOA have been observed in residential
wood burning smoke in both urban and rural environments as well (Brege et al., 2018; Kim et al., 2019; Stefania et al., 2016;
70   Sun et al., 2010). In addition, in remote regions where aerosols are generally highly aged and have been subjected to more
extensive aqueous-phase and heterogeneous processing, SOA is significantly more oxidized, less volatile, and more
hygroscopic compared to those in urban areas (Jimenez et al., 2009; Morgan et al., 2010; Ng et al., 2011; Zhang et al., 2011;
Zhou et al., 2019).

Understanding the chemical aging process of SOA in the aqueous phase is important for better predicting the concentration
75   of SOA in ambient air and assessing its potential impacts on climate and human health. Sunlight-triggered aqueous-phase
reactions, such as direct photolysis of organics, nitrate, nitrite, and hydrogen peroxide, as well as energy and charge-transfer
reactions driven by ^{3}C*, significantly impact the chemical aging of SOA, leading to changes in particle composition and
properties (Corral Arroyo et al., 2018; Ervens et al., 2011; Herrmann et al., 2015; Mabato et al., 2022). The extent of exposure
of aqSOA to oxidants in atmospheric waters can vary widely, influenced by the concentration and residence time of oxidants.
80   For example, the steady-state concentration of •OH can vary from 10^{-16} to 10^{-12} M (Herrmann et al., 2010) while that of ^{3}C*
can vary from 10^{-14} to 10^{-11} M (Kaur et al., 2019), depending on the solute concentration, which ranges from dilute fog/cloud
droplets to highly concentrated solutions in particle water. Exposure to elevated levels of oxidants can promote the formation
of highly oxygenated SOA (Daumit et al., 2016; Kang et al., 2011; Lambe et al., 2015; Ng et al., 2010), but can also decrease
SOA mass and facilitate a shift from the functionalization-dominant regime to the fragmentation-dominant regime (Lambe et
85   al., 2012).

This study focuses on the long-timescale aqueous aging of the aqSOA formed from the photooxidation of guaiacyl acetone
(GA). GA is commonly detected in the emissions from burning of plant-based biomaterials and has been used as a model
compound to study SOA formation in BB emissions. In our previous work (Arciva et al., 2022; Jiang et al., 2021b; Ma et al.,
2021; Misovich et al., 2021; Smith et al., 2016), we investigated the kinetics and mechanisms of aqSOA formation from the
90   photoreactions of GA. Here, we extend our research to investigate the photoreactions of GA with •OH and ^{3}C* and the
subsequent photooxidation of the resulting aqSOA in water. Our investigation is focused on studying the impact of prolonged
aqueous aging on the chemical composition and optical properties of the aqSOA. Specifically, we examine the effects of •OH
reaction and ^{3}C* reaction induced by simulated sunlight for up to 72 hours and 14 hours, respectively, which is equivalent to
approximately 21 days and 4 days of winter-solstice sunlight exposure in northern California. In addition, we also examine the
95   impact of light and additional oxidant exposure on the aging of the aqSOA.

2. Experimental Methods

2.1 Formation and Aging of Phenolic AqSOA

The initial reaction solution was prepared with 100 μM of guaiacyl acetone and either 100 μM of hydrogen peroxide (H_2O_2; as a source of •OH) or 5 μM of 3,4-dimethoxybenzaldehyde (3,4-DMB; as a source of $^3C^*$) in Milli-Q water. The pH of the solution was adjusted to 4.6 using sulfuric acid. These conditions were set to mimic wood burning-influenced cloud and fog waters (Jiang et al., 2021b). The reaction solution was placed in a 400 mL Pyrex tube, continuously stirred and illuminated inside a RPR-200 photoreactor system equipped with three different types of bulbs to roughly mimic sunlight (George et al., 2015). The steady-state concentration of •OH ([•OH]) is 2.6×10^{-15} M in the •OH-mediated reaction, similar to the values observed in fog water (Kaur and Anastasio, 2017), and the [$^3C^*$] is 1.1×10^{-13} M in the $^3C^*$-mediated reaction, about 2 times higher than in fog water (Kaur and Anastasio, 2018) (see Section 3.1 for more details). When ~95% of the initial GA has reacted (i.e., after 24 h of irradiation for the •OH reaction and 3.5 h for the $^3C^*$ reaction), the solution was separated into four aliquots and moved into separate 110 mL Pyrex tubes for further aging. This aging occurred under four different conditions: 1) aging in the dark (tube wrapped with aluminum foil); 2) continued illumination without the addition of extra oxidant; 3) photoaging with the addition of 100 μM of H_2O_2; and 4) photoaging with the addition of 5 μM of 3,4-DMB. Small aliquots of the solutions were then periodically taken from each tube to measure the chemical composition and optical properties.

2.2 Chemical and Optical Analyses

Concentrations of GA and 3,4-DMB were measured by a high-performance liquid chromatograph equipped with a diode array detector (HPLC-DAD, Agilent Technologies Inc.). The mass concentration and chemical composition of the aqSOA products were characterized using a high resolution time-of-flight aerosol mass spectrometer (HR-AMS; Aerodyne Res. Inc) after atomizing the liquid samples in argon (Ar, industrial grade, 99.997 %) followed by diffusion drying (Jiang et al., 2021b).

HR-AMS data were processed using standard toolkits (SQUIRREL v1.56D and PIKA 1.15D). Since Ar was used as the carrier gas, the CO^+ signal of aqSOA was quantified directly (Yu et al., 2016). While the organic H_2O^+ signal (org-H_2O^+) can also be directly determined for dry aerosols, it tends to be noisy due to high sulfate H_2O^+ (SO_4-H_2O^+) signal interference. Therefore, org-H_2O^+ was parameterized as org-$H_2O^+ = 0.4 \times CO_2^+$, based on the linear regression between the determined org-H_2O^+ signal (= measured-$H_2O^+ - SO_4$-H_2O^+) and the measured organic CO_2^+ signal (Jiang et al., 2021b). The other org-H_2O^+ related signals were parameterized as org-$OH^+ = 0.25 \times$org-H_2O^+ and org-$O^+ = 0.04 \times$org-H_2O^+ (Aiken et al., 2008). Atomic ratios of oxygen-to-carbon (O/C) and hydrogen-to-carbon (H/C), and organic mass-to-carbon ratio (OM/OC) ratios, were subsequently determined (Aiken et al., 2008), and the average oxidation state of carbon (OS_C) of aqSOA was calculated as $OS_C = 2 \times O/C$-H/C (Kroll et al., 2011). The aqSOA concentration in the solution ([Org]$_{solution}$, μg mL^{-1}) was calculated using sulfate as the internal standard:

$$[Org]_{solution} = [Org]_{AMS} \times \frac{[Sulfate]_{solution}}{[Sulfate]_{AMS}}$$

(Eq. 1)

where [Org]$_{AMS}$ and [Sulfate]$_{AMS}$ are the AMS-measured concentrations (µg m^{-3}) of aqSOA and sulfate in the aerosolized solution, and [Sulfate]$_{solution}$ is the spiked concentration (µg mL^{-1}) of sulfate in the solution. The aqSOA mass yield (Y_{SOA}) after a given time of illumination (t) was calculated as:

$$Y_{SOA} = \frac{[Org]_t}{[GA]_0 - [GA]_t}$$ (Eq. 2)

where [GA]$_0$ is the initial GA concentration (µg mL^{-1}) in the solution, and [Org]$_t$ and [GA]$_t$ denote the concentrations of GA and aqSOA, respectively, in the solution after a period of irradiation.

The light absorbance of the reaction solution was measured using a UV-Vis spectrophotometer (UV-2501PC, Shimadzu). The mass absorption coefficient, the absorption Ångström exponent, and the rate of sunlight absorption of the aqSOA were calculated (Section S1).

Positive matrix factorization (PMF) was performed on the combined matrix of the high-resolution mass spectra (*m/z* 12–360) and the UV-vis spectra (280–600 nm) of the •OH-aqSOA and ^{3}C*-aqSOA separately (Jiang et al., In prep). The PMF results were evaluated using the PMF Evaluation Toolkit (PET v3.08 downloaded from: http://cires1.colorado.edu/jimenez-group/wiki/index.php/PMF-AMS_Analysis_Guide). A three-factor solution with fPeak = 0 was chosen based on the evaluation criteria (Ulbrich et al., 2009; Zhang et al., 2011) for •OH- and ^{3}C*-aqSOA. Figures S1 and S2 summarize the diagnostic plots for the 3-factor PMF solutions for •OH- and ^{3}C*-aqSOA, respectively.

3. Results and Discussion

3.1 Formation and Characteristics of the aqSOA from Photooxidation of GA by •OH and ^{3}C*

Figures 1a and 1h demonstrate that the loss of GA follows first-order kinetics in both •OH- and ^{3}C*-mediated photoreactions. The fitted pseudo-first-order rate constants are 0.14 and 0.73 h^{-1}, respectively, under our experimental conditions. The fact that the reaction of GA with ^{3}C* is much faster than with •OH is consistent with previously reported kinetics for other phenols (Smith et al., 2014; Yu et al., 2016) and can be attributed to the higher oxidant concentration in the ^{3}C*-mediated reaction. Based on the second-order rate constants for GA reacting with •OH (1.5×10^{10} M^{-1} s^{-1}) (Arciva et al., 2022) and with ^{3}C* (1.8×10^9 M^{-1} s^{-1}) (Ma et al., 2021), we estimate that the steady-state concentrations of oxidants are: [•OH] = 2.6×10^{-15} M under the •OH-mediated reaction condition and [^{3}C*] = 1.1×10^{-13} M under the ^{3}C*-mediated reaction condition. These oxidant concentrations are comparable to previously observed values in fog waters ([•OH] ~ 2.0×10^{-15} M and [^{3}C*] ~ 5.0×10^{-14} M) (Kaur and Anastasio, 2017, 2018) and in water extracts of ambient particles ([•OH] ~ 4.4×10^{-16} M and [^{3}C*] ~ 1.0×10^{-13} M) (Kaur et al., 2019).
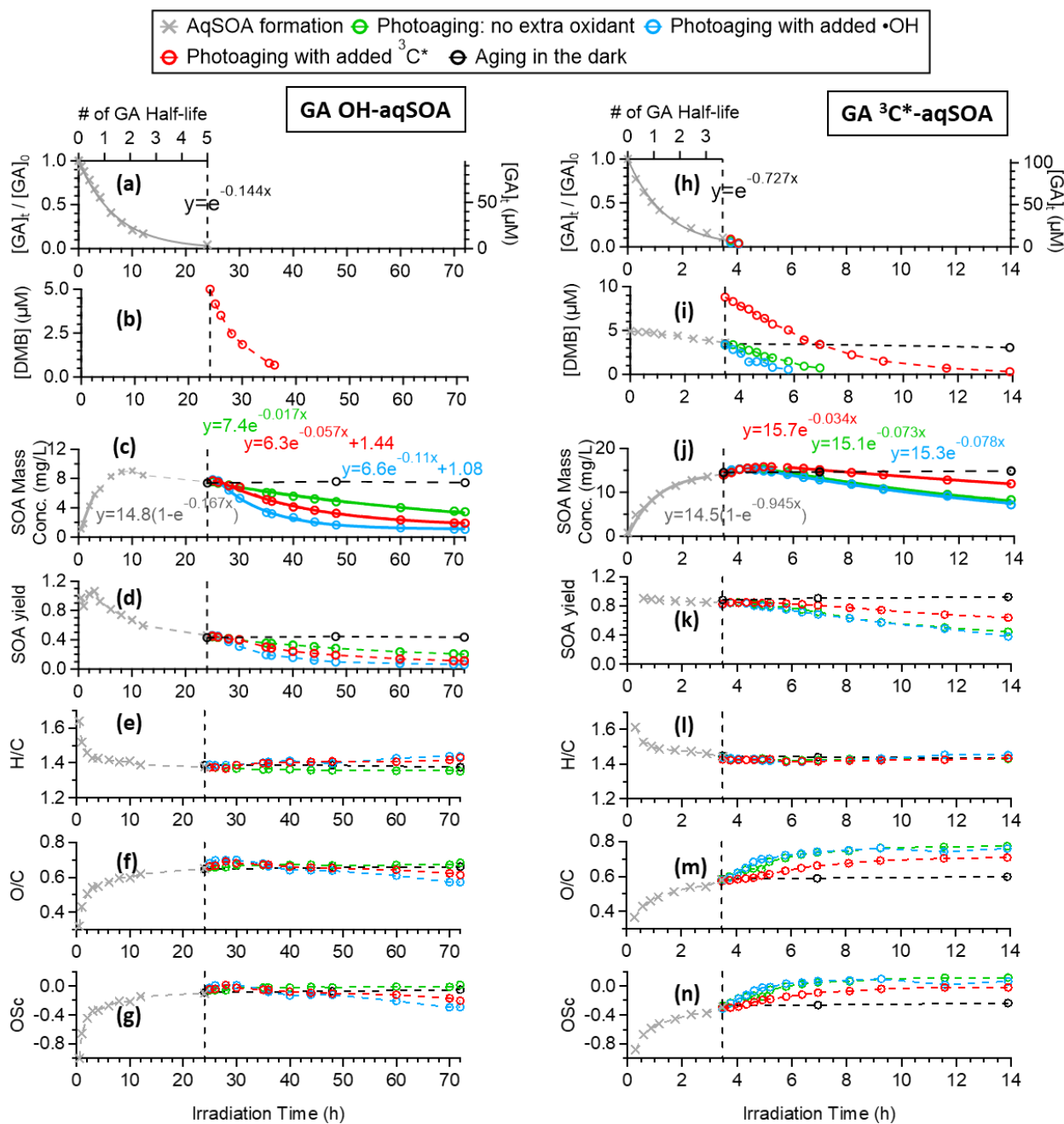
Figure 1. Overview of aqSOA formation and aging in •OH- and 3C*-initiated photoreactions of GA. Decay of (a & h) GA and (b & i) 3,4-DMB in the solution. Trends of aqSOA (c & j) mass concentration and (d & k) mass yield and (e & l) H/C, (f & m) O/C and (g & n) OSC determined by HR-ToF-AMS. These measured values are also shown in Tables S1 and S2.

As GA is transformed, the mass of the aqSOA increases (Figures 1c and 1j). For both •OH- and 3C*-mediated reactions, the aqSOA formation rate relative to the GA decay rate is similar initially, giving a relatively constant mass yield of ~ 90%

until one GA half-life ($t_{1/2}$, which is 4.8 h for the •OH reaction and 0.95 h for the ^{3}C* reaction). However, in the •OH reaction, the formation of aqSOA slows down after $t_{1/2}$, resulting in a reduction in SOA yield to as low as 46% when ~ 95% of the initial GA has reacted (Fig. 1d). In contrast, in the ^{3}C* reaction, the aqSOA yield stabilizes in the range of 85–90% until GA has been completely consumed (Figures 1d and 1k). These results suggest that the aqSOA reacts with •OH to produce volatile products, which leads to mass loss and slower mass growth. In addition, these results suggest that the •OH-aqSOA of GA is more vulnerable to photodegradation than is ^{3}C*-aqSOA, with a greater tendency to form volatile and semi-volatile compounds that evaporate from the condensed phase. This finding is confirmed by prolonged photoaging experiments, which are presented in Sections 3.2 and 3.4.

The chemical composition of GA aqSOA changes continuously during photoreaction. In both the •OH and ^{3}C* reactions, the O/C, OM/OC, and OS_C of the aqSOA increase, while H/C slightly decreases until all the GA has been consumed (Figures 1e-g and l-n). The HR-AMS spectra of the aqSOA (Figures 2a and 2b) show that when ~95% of the initial GA has reacted (at 24 h for the •OH reaction and 3.5 h for the ^{3}C* reaction), the •OH-aqSOA (O/C = 0.64 and OS_C = −0.10) is more oxidized than the ^{3}C*-aqSOA (O/C = 0.56 and OS_C = −0.29). In addition, compared with the •OH-aqSOA, the ^{3}C*-aqSOA spectrum shows a significantly greater abundance of high m/z ions (Figures 2c-e), including the marker ions of GA oligomers (e.g., $C_{18}H_{19}O_5^+$ and $C_{20}H_{22}O_6^+$ at m/z 315 and 358, respectively) (Jiang et al., 2021b), suggesting a higher production of oligomers with ^{3}C*. This observation aligns with the trend we observed previously in the aqueous-phase oxidations of phenol and methoxyphenols, where more oligomerization occurred in photoreactions initiated by ^{3}C*, while •OH reactions promoted the breakdown of aromatic rings and formation of smaller organic acids (Sun et al., 2010; Yu et al., 2014).
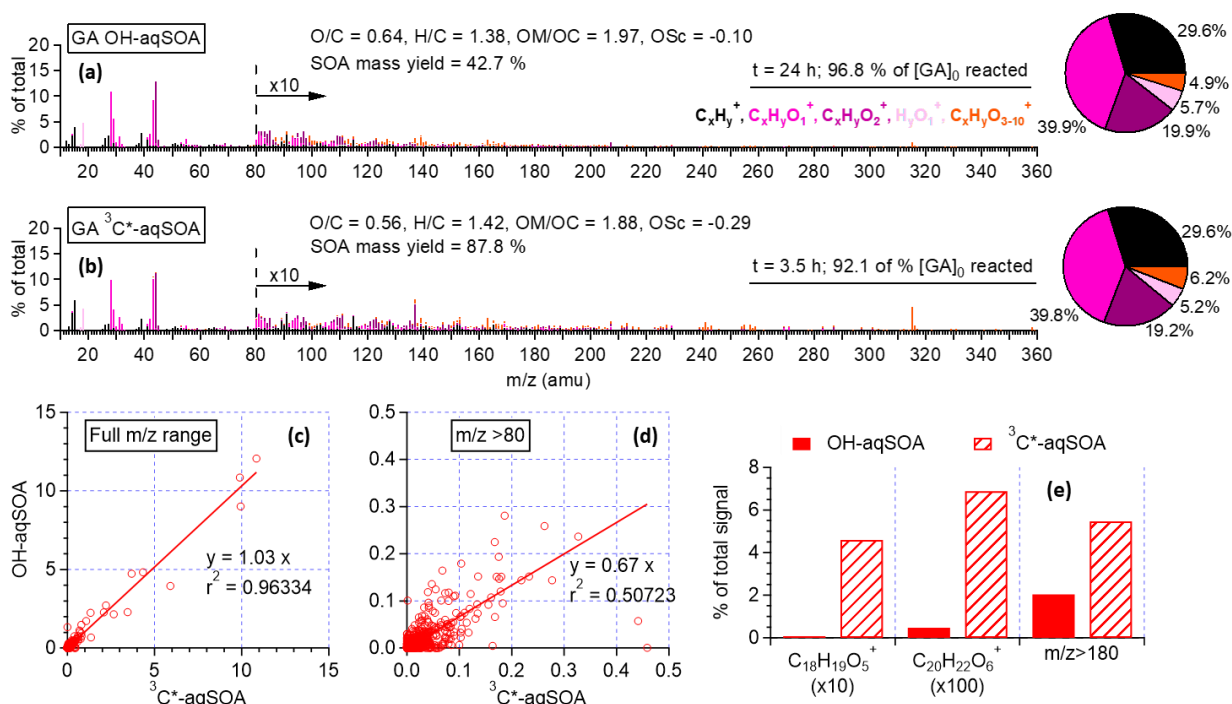
Figure 2. HR-AMS mass spectra of (a) •OH-aqSOA and (b) ³C*-aqSOA after nearly all the initial GA has reacted. Scatter plots that compare the mass spectra of the •OH-aqSOA with ³C*-aqSOA for (c) all ions and for (d) ions with m/z > 80. (e) Relative abundances of the GA-oligomer tracer ions and high mass ions (m/z>180) in the HR-AMS spectra of the aqSOA.

The compositional differences between the •OH-aqSOA and ³C*-aqSOA may be explained by the different reaction mechanisms. In the •OH experiment, the reaction can start either by •OH-addition to the aromatic ring to generate OH-adducts or by H-atom abstraction from the hydroxyl group to generate a phenoxy radical. The subsequent coupling of phenoxy radicals leads to the formation of oligomers (Kobayashi and Higashimura, 2003). According to previous studies (Atkinson, 1986; Olariu et al., 2002), at room temperature, only ~10% of the phenol + •OH reaction results in H-atom abstraction to form phenoxy radical, whereas ~90% of the •OH reaction proceeds through OH addition. On the other hand, the ³C* reaction primarily proceeds through electron transfer and/or H-atom abstraction which produces a phenoxy radical (Anastasio et al., 1997; Canonica et al., 2000; Yu et al., 2014). The more pronounced production of phenoxy radicals in the ³C* reaction can lead to more prominent oligomerization. Although the reactions of phenols with ³C* also produce •OH radical, the amount generated is relatively small (Anastasio et al., 1997; Smith et al., 2014) and the •OH addition pathway in the ³C* reaction is expected to be less important than in the •OH reaction.

Figures 3d and 3j (and Figures S3a and S4a) show the mass absorption coefficient spectra of the •OH-aqSOA and the ³C*-aqSOA. Both aqSOAs are more light-absorbing than the parent GA (Figure S5), which is likely due to the formation of GA oligomers and functionalized products containing conjugated structures. Phenolic dimers and higher oligomers formed through the coupling of phenoxyl radicals and monomeric phenol derivatives formed through •OH and carbonyl addition to the aromatic ring are effective light absorbers (Jiang et al., 2021b; Misovich et al., 2021; Yu et al., 2014). In addition, the ³C*-aqSOA exhibits greater light absorption than the •OH-aqSOA for a similar extent of GA decay, reflecting the fact that the ³C*-aqSOA is generally enriched with more high-molecular-weight conjugated species.
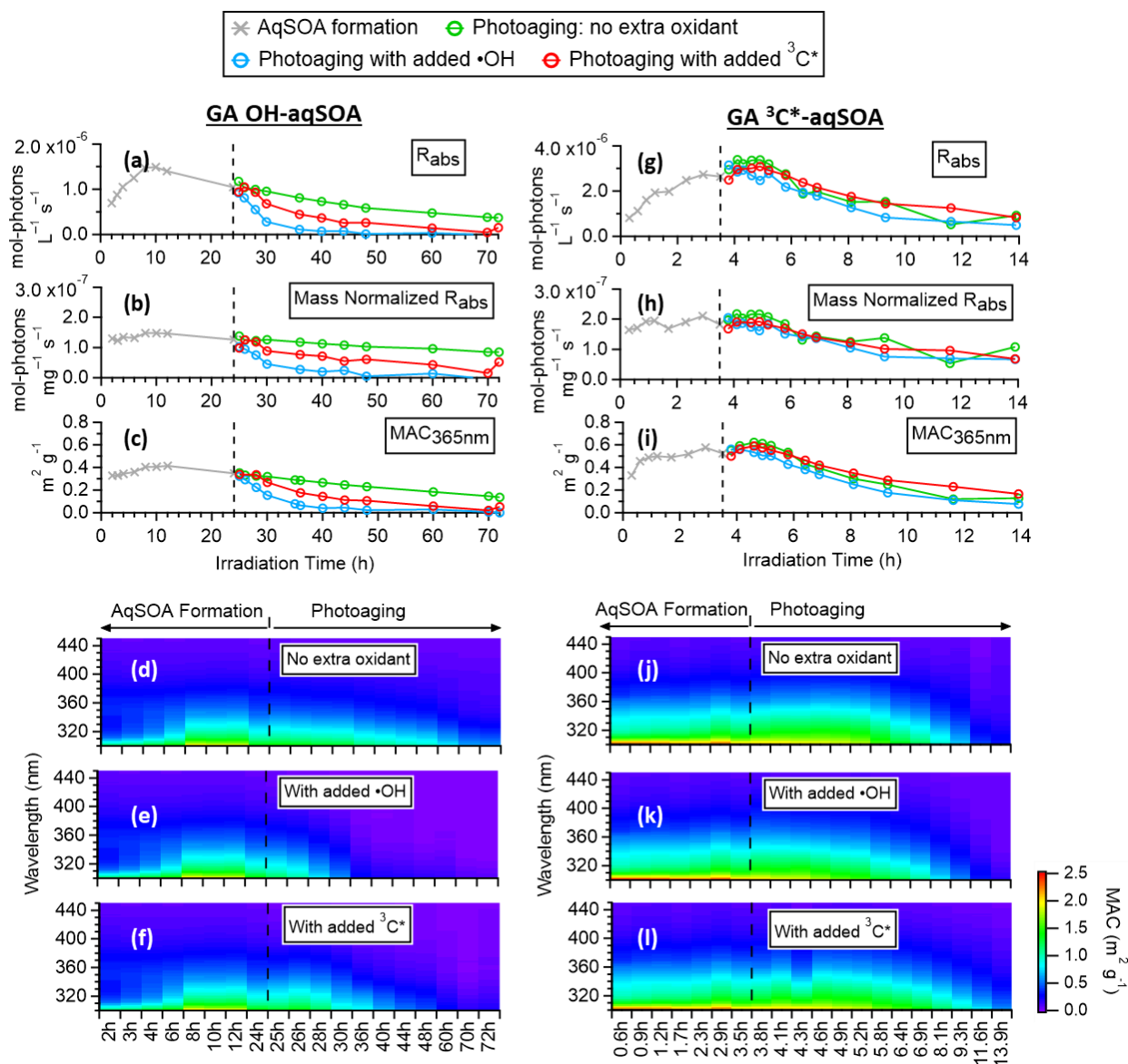
Figure 3. Evolution of the optical properties of •OH-aqSOA and ³C*-aqSOA during the course of the photoreactions: (a & g) rate of sunlight absorption; (b & h) rate of sunlight absorption normalized by aqSOA mass; (c & i) mass absorption coefficient (MAC) at 365 nm; and (d-f & j-l) MAC spectra in the wavelength range of 300-450 nm.

3.2 Photo-transformation of AqSOA and Influence of Prolonged Photoaging on SOA Yield and Composition

After ~95% of the initial GA has reacted, the aqSOA was subjected to additional aging under different conditions: 1) aging in the dark; 2) continued illumination without the addition of extra oxidant; and 3) continued illumination with the addition of an oxidant (•OH or ³C*). As shown in Figures 1c-g, 1j-n, and S6, the mass concentration, elemental ratios, and

HR-AMS spectra of the aqSOA remain unchanged during dark aging, indicating negligible dark chemical reactions. In contrast, continued exposure to simulated sunlight results in a 46% reduction in the mass of ^{3}C*-aqSOA over about 10 hours of prolonged aging. More than 60% of the •OH-aqSOA mass is degraded after 48 hours of extended photoaging (i.e., 72 hours of irradiation in total). These observations indicate that phenolic aqSOA is susceptible to photodegradation and that fragmentation reactions and evaporation of volatile products likely play important roles in the photoaging process. Furthermore, the fitted pseudo-first-order decay rate constant (k) is 0.073 h^{-1} for the ^{3}C*-aqSOA and 0.017 h^{-1} for the •OH-aqSOA (Figures 1c, 1j, and 4). The faster decay of the ^{3}C*-aqSOA is likely due to the higher oxidant concentration in the ^{3}C* reaction during aqSOA aging. Here, we assume the steady-state concentrations of •OH and ^{3}C* at the onset of the prolonged photoaging are approximately the same as in the initial solutions, and thus the [^{3}C*] in the ^{3}C* reaction is about 40 times higher than the [•OH] in the •OH reaction during aqSOA aging. This assumption is proved by the first-order decay behavior of GA and the relatively stable 3,4-DMB concentration during the aqSOA formation period. Additionally, •OH production from ^{3}C* becomes increasingly important in the prolonged photoaging and it may lead to increased oxidant concentration in the ^{3}C* solution. Another possible reason for the faster decay of the ^{3}C*-aqSOA may be explained by its higher light absorptivity which leads to faster direct photodegradation.
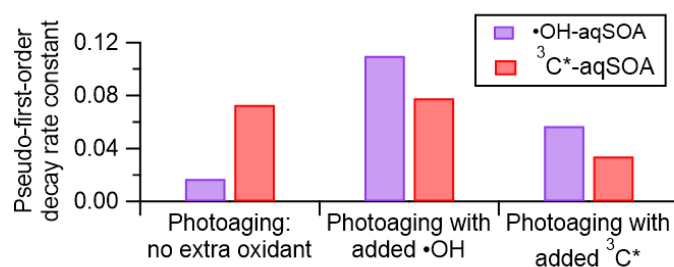
Figure 4. Pseudo-first-order decay rate constants for loss of mass of •OH-aqSOA and ^{3}C*-aqSOA under different photoaging conditions

As depicted in Figures 1l-n and S7, the chemical composition of ^{3}C*-aqSOA evolves continuously during photoaging, with the O/C ratio increasing from 0.59 to 0.77, consistent with previous research demonstrating that SOA becomes more oxidized during chemical aging (Kroll et al., 2015; Yu et al., 2016). In contrast, the O/C and H/C ratios of •OH-aqSOA exhibit negligible changes (O/C = 0.67±0.008 and H/C = 1.36±0.008) during prolonged photoaging (Figures 1e-g and S7), even though the mass of aqSOA decreases significantly. This can be explained by the simultaneous evaporation of highly oxidized volatile compounds and the transformation of less oxidized species into more oxidized, low-volatility products, thereby maintaining relatively constant bulk elemental ratios. Additionally, as shown in Figures 5, S8, and S9, both •OH-aqSOA and ^{3}C*-aqSOA show increasing f$_{CHO2+}$ (mass fraction of CHO$_2^+$ in the AMS spectrum; a tracer of carboxylic acids) and decreasing f$_{C2H3O+}$ (mass fraction of C$_2$H$_3$O$^+$ in the AMS spectrum; a tracer of non-acid carbonyls) during prolonged photoaging, indicating the importance of acid formation in the aqSOA. The more significant increase of f$_{CHO2+}$ in the ^{3}C*-aqSOA compared to •OH-

235 aqSOA during aging suggests that acid formation is more pronounced in the aging of the ^{3}C*-aqSOA, although it is important

for both •OH-aqSOA and the ^{3}C*-aqSOA during the initial SOA formation.
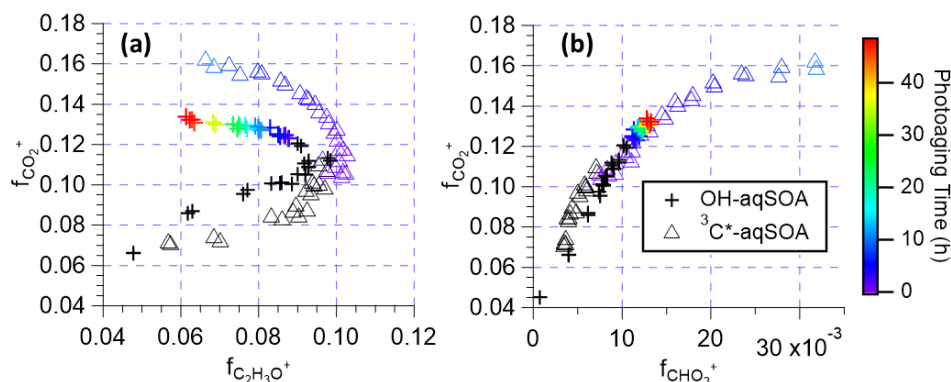
Figure 5. The plots of f$_{CO2+}$ vs. f$_{C2H3O+}$ and f$_{CO2+}$ vs f$_{CHO2+}$ that illustrate the evolution of the •OH-aqSOA and ^{3}C*-aqSOA during the formation and the prolonged photoaging periods under the condition of no extra oxidant addition. The black markers represent the
240 **period of aqSOA formation, while the colored markers represent prolonged aqSOA aging (i.e., after ~95% of the initial GA is consumed).**

To further elucidate the chemical evolution of the aqSOA, we performed PMF analysis on the combined AMS and UV–

vis absorption spectral data and successfully resolved three distinct factors for both •OH-aqSOA and ^{3}C*-aqSOA, each with

different temporal profiles, mass spectra, and absorption spectra that represent different generations of aqSOA products

245 (Figures 6 and 7). The first-generation ^{3}C*-aqSOA, which is the least-oxidized (O/C=0.49 and H/C=1.48), shows enhanced

ion signals corresponding to GA oligomers, such as $C_{18}H_{19}O_5^+$ and $C_{20}H_{22}O_6^+$ (Figures 7a, 7j, 7k and S11e-f). These products

grow rapidly and peak within the first hour of ^{3}C*-aqSOA formation, but they subsequently decrease and disappear completely

when GA is consumed. The second-generation factor (O/C=0.59 and H/C=1.42), in which the oligomer tracer ions are

substantially reduced, shows enhanced ion signals corresponding to functionalized GA monomers or ring-opening dimers such

250 as $C_9H_7O_3^+$ and $C_{15}H_{11}O_4^+$ (Figures 7b, 7j, 7k and S11d). The second-generation products build up gradually, peak after GA

is consumed, and degrade more slowly than the 1st-generation ^{3}C*-aqSOA (k = 0.36 h^{-1} vs 1.8 h^{-1}) during prolonged aging

(Figure 7d).
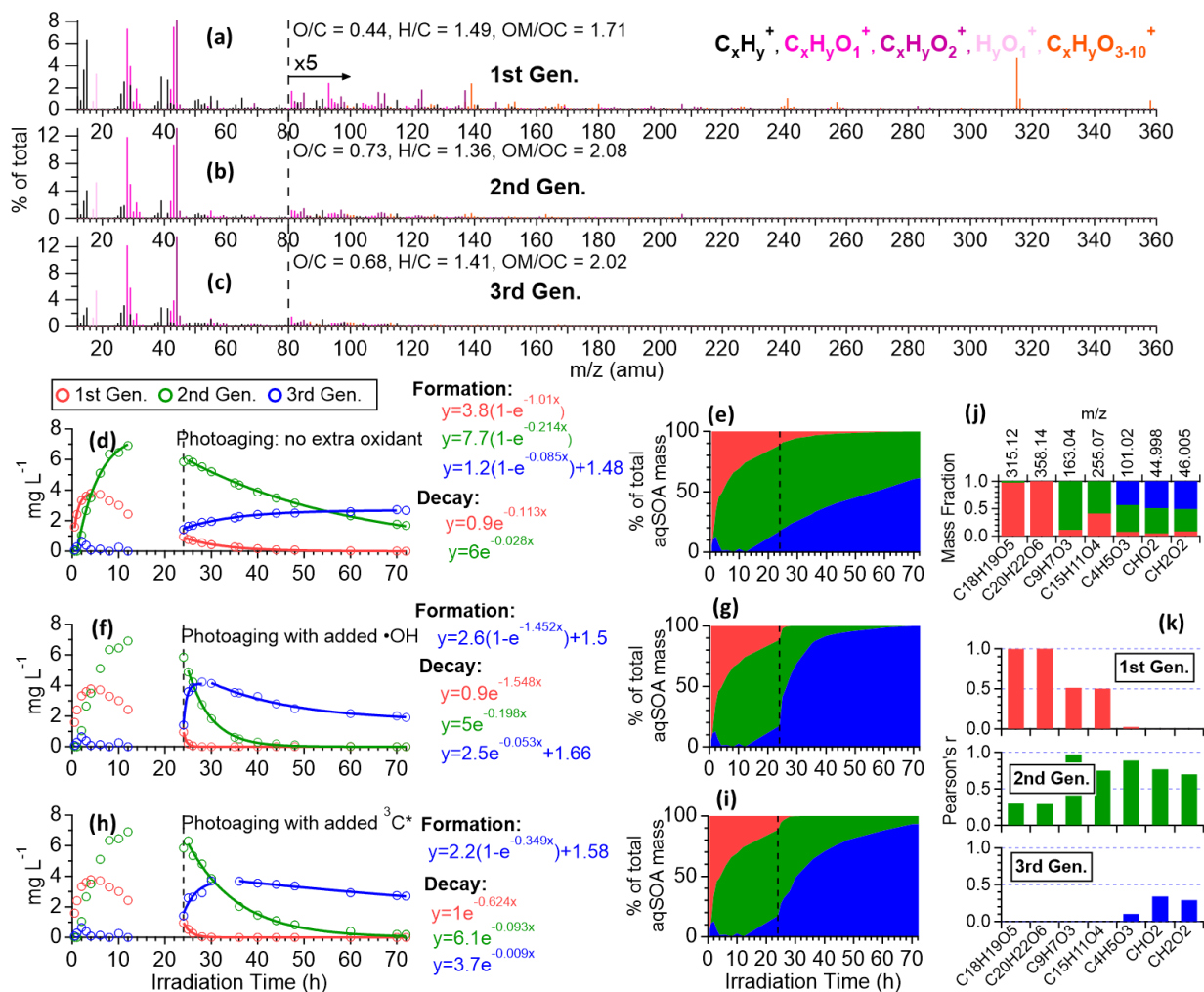
Figure 6. Characteristics of the three generations of the •OH-aqSOA products resolved by PMF: (a-c) MS profiles; (d, f, and h) mass concentration time series; and (e, g, and i) fractional contribution time series of the PMF factors. (j) Mass fraction of selected AMS tracer ions attributed to each PMF factor. (k) Correlation between PMF factors and selected AMS tracer ions.
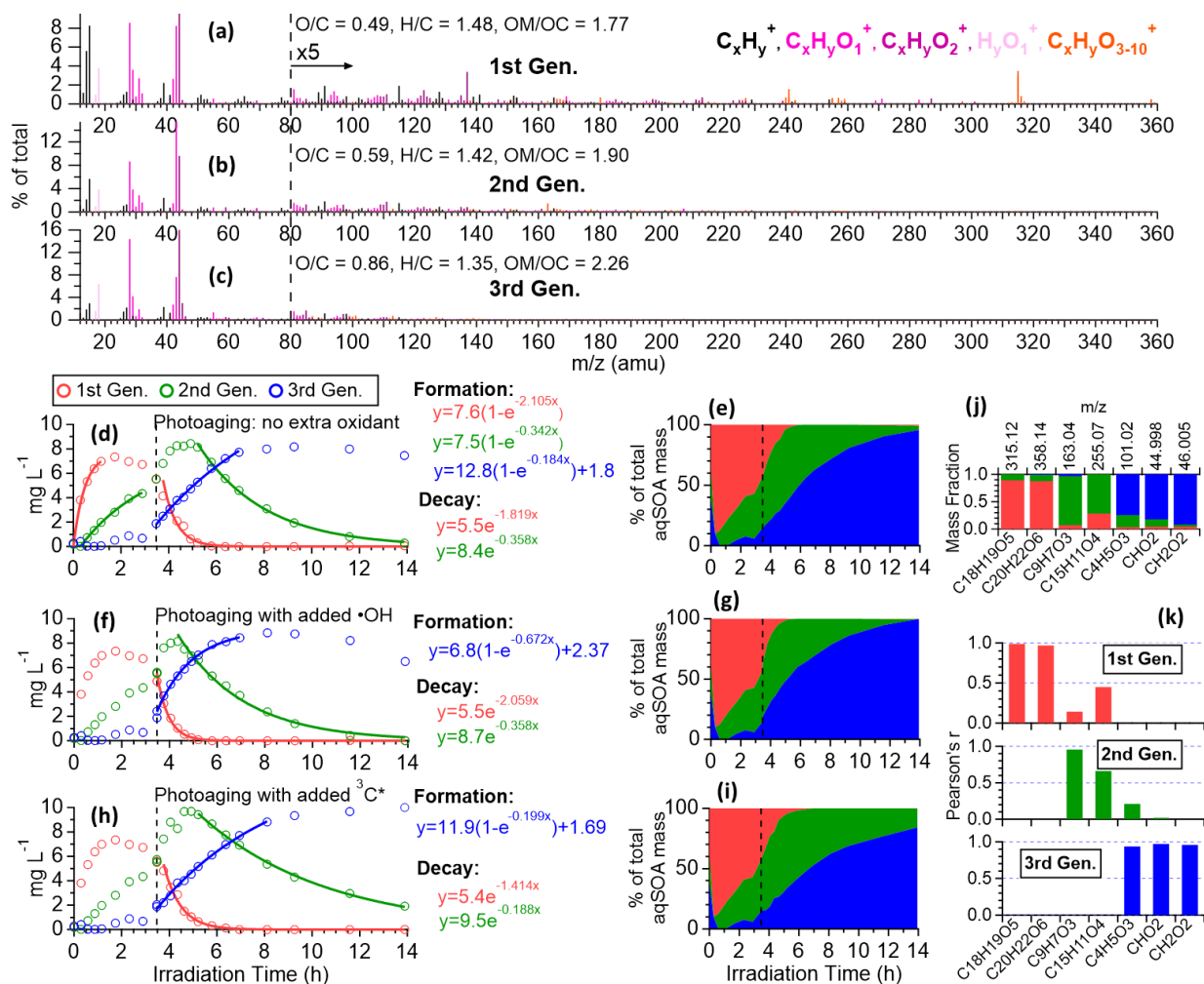
Figure 7. Characteristics of the three generations of the ^{3}C*-aqSOA products resolved by PMF: (a-c) MS profiles; (d, f, and h) mass concentration time series; and (e, g, and i) fractional contribution time series of the PMF factors. (j) Mass fraction of selected AMS tracer ions attributed to each PMF factor. (k) Correlation between PMF factors and selected AMS tracer ions.

The third-generation factor of ^{3}C*-aqSOA is the most oxidized (O/C = 0.86 and H/C = 1.36), and its mass spectrum shows negligible high m/z signals but elevated small, oxygenated ions such as CHO_2^+, $CH_2O_2^+$, and $C_4H_5O_3^+$ (Figures 7c, 7j, 7k and S11a-c). The increase of this factor is observed when the 1st-generation factor starts to decline. It continues to increase but shows a slight decrease towards the end of prolonged photoaging. These findings agree with our previous studies, which demonstrate that oligomerization and functionalization play a more significant role in the initial formation of phenolic aqSOA, while fragmentation and ring-opening reactions to produce more oxidized compounds become more important later (Jiang et al., 2021b; Yu et al., 2016). Further, the observed decay of the 3rd-generation aqSOA indicates that prolonged aging leads to

the formation of volatile compounds that evaporate from the condensed phase, resulting in mass loss of aqSOA. This implies that photochemical aging can remove aqSOA from the atmosphere, in addition to wet and dry deposition (Hodzic et al., 2016).

270   The mass spectral features of the •OH-aqSOA factors (Figures 6a-c) are generally similar to those of the ^{3}C*-aqSOA factors (Figures 7a-c). However, in •OH-aqSOA, we observed that the 2nd-generation (O/C = 0.73 and H/C = 1.36) is the most oxidized factor and shows strong correlations not only with the tracer ions representing functionalized GA monomers (e.g., $C_9H_7O_3^+$ and $C_{15}H_{11}O_4^+$) but also with a group of small, oxygenated ions (e.g., CHO_2^+, $CH_2O_2^+$, and $C_4H_5O_3^+$) that are enriched in the 3rd-generation ^{3}C*-aqSOA. These results suggest that •OH reaction tends to form highly oxidized products that degrade

275   over long aging times, whereas the ^{3}C* reaction can generate highly oxidized SOA products that are more resistant to degradation. Another possible explanation is that the highly oxidized species in the aqSOA are less reactive with ^{3}C* than with •OH, and thus they can persist in the aqueous phase in the ^{3}C* reaction, while •OH is able to further oxidize these highly oxidized products and eventually transform them into volatile species. This explanation is supported by the more significant decay of the 3rd-generation ^{3}C*-aqSOA when extra H_2O_2 is added during prolonged photoaging (Figures 7d and 7f). In

280   addition, compared to ^{3}C*-aqSOA, •OH-aqSOA exhibits much lower production of 1st-generation products but higher 2nd-generation (Figures 7d-e vs. Figures 6d-e), suggesting that oligomerization is more pronounced in ^{3}C*-aqSOA, while functionalization plays a more important role in •OH-aqSOA.

3.3 Evolution of AqSOA Optical Properties during Prolonged Aging

Figures 3, S3, and S4 illustrate the evolution of the light absorption properties of the aqSOA during formation and aging.

285   The aqSOA experiences photobleaching during prolonged aging, with the MAC$_{365nm}$ value of the •OH-aqSOA decreasing from 0.41 (the maximum) to 0.14 m^2 g^{-1}, and that of ^{3}C*-aqSOA decreasing from 0.62 (the maximum) to 0.13 m^2 g^{-1}. The rates of sunlight absorption, both normalized and un-normalized by aqSOA mass, also decrease during prolonged aging. Figure 8 displays the AAE of the aqSOA as a function of $\log_{10}$(MAC$_{405}$) and an optical-based classification of BrC (Saleh, 2020; Zhai et al., 2022). As a result of prolonged photoaging, the GA aqSOA shifts from being classified as weak BrC to very weak BrC.

290   The changes in the light absorption properties of the GA aqSOA are also influenced by elevated oxidant concentrations (see Section 3.4 for further discussions).
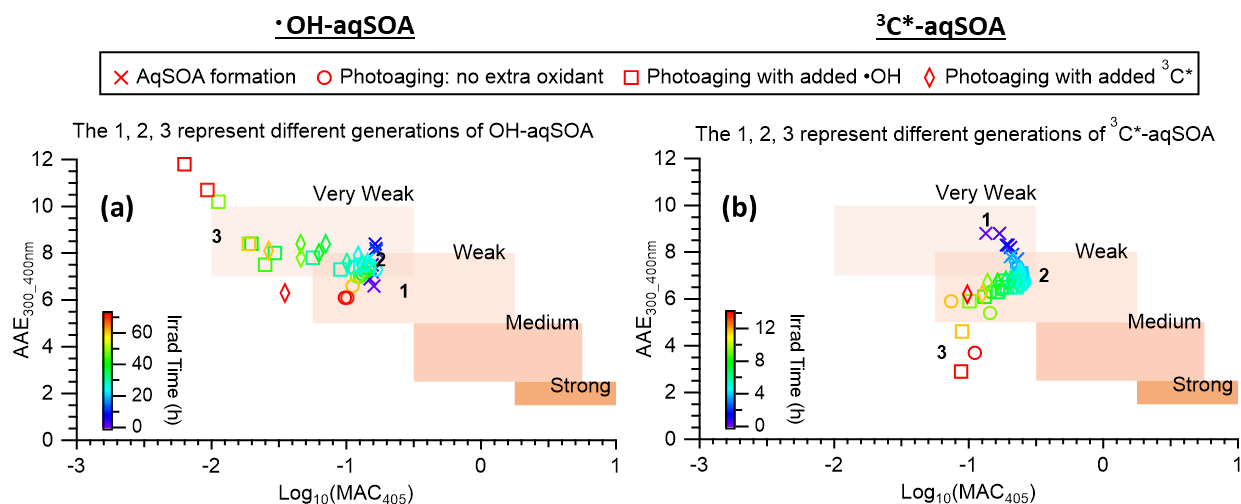
Figure 8. The light absorption properties of (a) •OH-aqSOA and (b) ³C*-aqSOA as shown in the AAE vs. log₁₀(MAC₄₀₅) space. The shaded areas in each plot represent very weakly, weakly, moderately, and strongly absorbing BrC denoted based on the optical-based BrC classification scheme (Saleh, 2020; Zhai et al., 2022). The numbers 1, 2, and 3 represent the different generations of the •OH-aqSOA and the ³C*-aqSOA products obtained from PMF.

Figure 9 presents the mass absorption coefficient spectra resolved by PMF for the three generations of GA aqSOA resulting from •OH and ³C* reactions. In general, the ³C*-aqSOA factors are more light-absorbing than the •OH-aqSOA factors, which is consistent with the higher abundance of oligomers and conjugated high molecular weight products in the ³C*-aqSOA. The 1st-generation aqSOA factor exhibits a hump in the MAC spectra between 340 and 400 nm, a feature observed previously in phenolic aqSOA (Smith et al., 2016) and attributed to the high conjugation present in oligomeric products. For both •OH- and ³C*-mediated reactions, the intermediate, 2nd-generation aqSOA are the most light-absorbing compared to the fresher (i.e., 1st-generation) and more aged (i.e., 3rd-generation) aqSOA. However, the 2nd-generation •OH-aqSOA exhibits relatively lower MAC values (MAC_{365nm} = 0.47 m² g⁻¹) than the 2nd-generation ³C*-aqSOA (MAC_{365nm} = 0.89 m² g⁻¹), possibly due to its higher oxidation degree, which can lead to the destruction of chromophores. The 3rd-generation aqSOA factors are the least absorbing (MAC_{365nm} = 0.070 m² g⁻¹ for the •OH-aqSOA and 0.018 m² g⁻¹ for the ³C*-aqSOA), consistent with the dominance of fragmented and ring-opening products in prolonged aging.
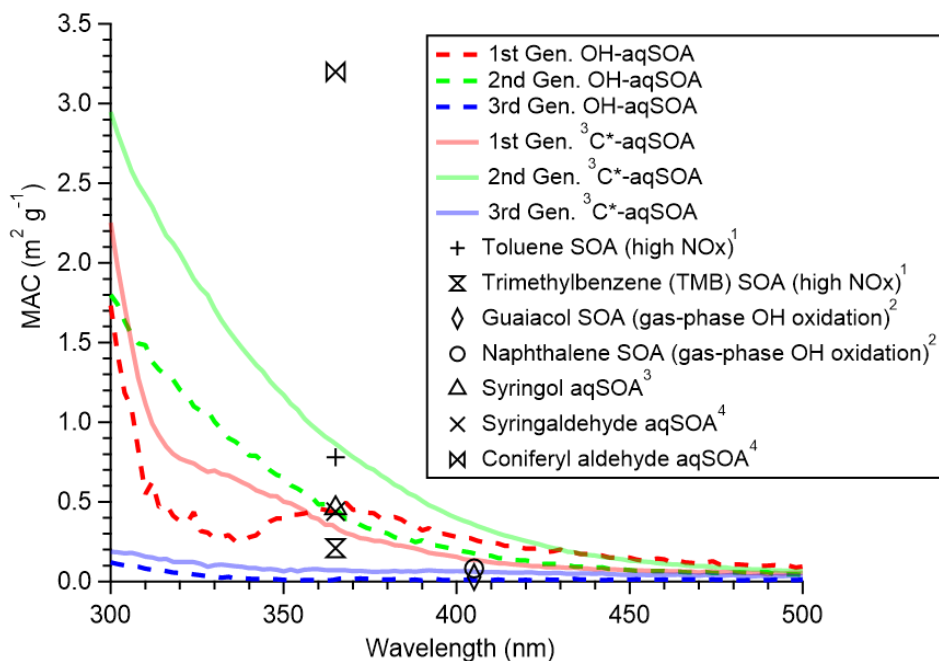
Figure 9. Mass absorption coefficient spectra of the PMF resolved three generations of the OH-aqSOA and the [3]C*-aqSOA, comparing with previously reported MAC values of SOA produced from aromatic precursors by [1] Liu et al., 2016, [2] Lambe et al., 2013,[3] Yu et al., 2014 and [4] Smith et al., 2016.

3.4 Effects of Additional Oxidant Exposure on AqSOA Aging

To investigate the effect of the concentrations of condensed-phase oxidants on the photoaging of phenolic aqSOA, we added either 100 µM H_2O_2 or 5 µM 3,4-DMB into the solution after the majority (~ 95 %) of GA had reacted. Since GA decay follows first-order kinetics, we assumed that the steady-state concentration of oxidants remained constant during initial aqSOA formation. By introducing additional H_2O_2 or 3,4-DMB, we increased the •OH or $^3C^*$ concentration, as well as the overall oxidant concentration in the solution during the photoaging of the aqSOA.

As shown in Figures 1c and 4 and Table S3, compared to continued photoaging with no addition of extra oxidant ($k = 0.017$ h^{-1}), the photodegradation rates of •OH-aqSOA are substantially faster when extra •OH or $^3C^*$ are introduced ($k = 0.11$ and 0.057 h^{-1}, respectively). As shown in Figures 6d, 6f, and 6h, the decay of the 1st- and 2nd-generation •OH-aqSOA is increased, and concurrently, the formation of the 3rd-generation factor is accelerated when extra oxidants are introduced, suggesting a faster transformation from the 1st to 2nd to 3rd generation. In addition, in the later stage of photoaging, we observed a more significant decay of the 3rd-generation •OH-aqSOA when extra oxidants are added, which suggests that higher concentrations of oxidants also facilitate the ultimate breakdown of the 3rd-generation •OH-aqSOA. The O/C and OSc of •OH-aqSOA exhibit a slightly faster increase upon the addition of extra •OH or $^3C^*$, but eventually decrease more

significantly by the end of the photoaging (Figures 1f and 1g), indicating accelerated formation of highly oxidized species and enhanced production of volatile compounds under high oxidant concentrations. Furthermore, increased oxidant concentrations also have significant impacts on the photobleaching of •OH-aqSOA. Specifically, the MAC values of the aqSOA decrease

330   faster when extra oxidants are added (Figure 3c-f). It is noteworthy that the addition of 100 µM of H_2O_2, the source of •OH, has a greater impact on the degradation of •OH-aqSOA mass and light absorption than the addition of 5 µM of 3,4-DMB, the source of $^3C^*$, despite the fact that the GA reaction with $^3C^*$ is much faster than that with •OH in this study. This result may reflect the reactivity differences between GA and the aqSOA with the oxidants, i.e., while both oxidants react quickly with phenolic compounds (e.g., GA), for other types of organics (e.g., the non-phenolic products in the aqSOA), •OH generally

335   reacts much more rapidly than do triplets. Another possible interpretation is that the addition of 3,4-DMB into the solution during aqSOA aging produces unique low-volatility, light-absorbing products which cannot be generated in •OH reactions. These products may counteract some of the mass and absorption loss due to fragmentation and evaporation.

Elevated oxidant concentrations also affect the photoaging of $^3C^*$-aqSOA. Unlike •OH-aqSOA, the addition of •OH during aging only slightly accelerates the decrease of mass and light absorption of the $^3C^*$-aqSOA (Figure 1j-k and Figure 3g-l). One

340   possible explanation is that the added •OH only accounts for a small fraction of the total oxidant amount in the $^3C^*$-initiated reaction system, and thus shows little impact on the aqSOA aging compared to the preexisting oxidants (e.g., $^3C^*$ and •OH generated from $^3C^*$). Another possible explanation is that the added •OH reacts with 3,4-DMB in the solution, resulting in a decrease in the amount of $^3C^*$ source. Additionally, the reaction of •OH with 3,4-DMB may also generate low-volatility products that balance out the increased decay of the aqSOA. This interpretation is consistent with the fast decay of 3,4-DMB

345   after the addition of extra •OH (Figure 1i). However, when extra $^3C^*$ (i.e., 3,4-DMB) is added to the $^3C^*$-aqSOA solution during extended aging, it slows down the decay of $^3C^*$-aqSOA mass and light absorption due to the enhanced formation of 2nd-generation products (Figure 7h vs. Figure 7d). This suggests that an increase in $^3C^*$ concentration during aging promotes the formation of low-volatility functionalized products.

Conclusions

350   This study investigates the evolution of the composition and optical properties of phenolic aqSOA during prolonged photoaging, including the effects of increased oxidant concentrations. The aqSOA was generated by reacting GA with •OH or $^3C^*$ under relatively dilute cloud/fog water conditions. Compared to the •OH reaction, the $^3C^*$ reaction is significantly faster, and leads to higher mass yields of aqSOA, more oligomers, and increased high molecular-weight species when the same fraction of initial GA has reacted. On the other hand, the •OH reaction generates aqSOA that is more oxidized and more

355   enriched in small, highly oxygenated species. Consistent with their compositional differences, the $^3C^*$-aqSOA is more light-absorbing than the •OH-aqSOA.

The chemical composition of the aqSOA evolves during photoaging, with oligomerization and functionalization being the dominant mechanisms during initial aqSOA formation, while fragmentation and volatile product formation becoming more

important during prolonged aging. This leads to a loss of 62–88% of the •OH-aqSOA mass after 48 hours of prolonged aging
under simulated sunlight with or without added oxidants, while the ^{3}C*-aqSOA experienced a loss of 25–54% of its mass after
10.5 hours of extended photoaging. These results suggest that aqueous-phase photochemical aging can remove atmospheric
aqSOA, in addition to wet and dry deposition. The average oxidation state of the ^{3}C*-aqSOA increases continuously during
photoaging, while that of •OH-aqSOA exhibits a slight decrease towards the end of photoaging when additional oxidants are
introduced; this is likely due to the formation and evaporation of highly oxidized volatile products. This finding indicates that
photoaging does not necessarily increase the average oxidation state of condensed-phase organics, as the evaporation of highly
oxidized products may decrease the average O/C of aqSOA. As photoaging continues, photobleaching becomes more
pronounced, causing the aqSOA to shift from weakly absorbing BrC to very weak BrC. According to PMF analysis, the second-
generation aqSOA, which is enriched in functionalized phenolic compounds, is the most light-absorbing. Elevated oxidant
concentrations during photoaging promote fragmentation reactions over oligomerization and functionalization reactions and
can ultimately promote the breakdown and evaporation of the aqSOA products, resulting in a faster decline in aqSOA mass
and light absorption.

Acknowledgments

This research was supported by grants from the National Science Foundation (NSF) (Grant #AGS-2220307), the U.S.
Department of Energy (DOE) Atmospheric System Research Program (Grant #DESC0022140), and the California Agricultural
Experiment Station (Projects CA-D-ETX-2102-H and CA-D-LAW-6403-RR). W.J. also acknowledges funding from the
Fumio Matsumura Memorial Fellowship by the Department of Environmental Toxicology at the University of California at
Davis.

Author contributions

QZ and WJ developed the research goals and designed the experiments. WJ and CN performed the experiments. WJ and QZ
analyzed the data and prepared the manuscript with contributions from all co-authors.

Competing interests

The contact author has declared that none of the authors has any competing interests.

Reference

Aiken, A. C., DeCarlo, P. F., Kroll, J. H., Worsnop, D. R., Huffman, J. A., Docherty, K. S., Ulbrich, I. M., Mohr, C., Kimmel,
J. R., Sueper, D., Sun, Y., Zhang, Q., Trimborn, A., Northway, M., Ziemann, P. J., Canagaratna, M. R., Onasch, T. B.,

Alfarra, M. R., Prevot, A. S. H., Dommen, J., Duplissy, J., Metzger, A., Baltensperger, U. and Jimenez, J. L.: O/C and OM/OC Ratios of Primary, Secondary, and Ambient Organic Aerosols with High-Resolution Time-of-Flight Aerosol Mass Spectrometry, Environ. Sci. Technol., 42(12), 4478–4485, doi:10.1021/es703009q, 2008.

390 Anastasio, C., Faust, B. C. and Rao, C. J.: Aromatic Carbonyl Compounds as Aqueous-Phase Photochemical Sources of Hydrogen Peroxide in Acidic Sulfate Aerosols, Fogs, and Clouds. 1. Non-Phenolic Methoxybenzaldehydes and Methoxyacetophenones with Reductants (Phenols), Environ. Sci. Technol., 31(1), 218–232, doi:10.1021/es960359g, 1997.

Arciva, S., Niedek, C., Mavis, C., Yoon, M., Sanchez, M. E., Zhang, Q. and Anastasio, C.: Aqueous ·OH Oxidation of Highly Substituted Phenols as a Source of Secondary Organic Aerosol, Environ. Sci. Technol., 56(14), 9959–9967, doi:10.1021/acs.est.2c02225, 2022.

395 Atkinson, R.: Kinetics and mechanisms of the gas-phase reactions of the hydroxyl radical with organic compounds under atmospheric conditions, Chem. Rev., 86(1), 69–201, doi:10.1021/cr00071a004, 1986.

Berndt, T. and Böge, O.: Formation of phenol and carbonyls from the atmospheric reaction of OH radicals with benzene, Phys. Chem. Chem. Phys., 8(10), 1205–1214, doi:10.1039/B514148F, 2006.

Brege, M., Paglione, M., Gilardoni, S., Decesari, S., Facchini, M. C. and Mazzoleni, L. R.: Molecular insights on aging and
400 aqueous-phase processing from ambient biomass burning emissions-influenced Po Valley fog and aerosol, Atmos. Chem. Phys., 18(17), 13197–13214, doi:10.5194/acp-18-13197-2018, 2018.

Bruns, E. A., El Haddad, I., Slowik, J. G., Kilic, D., Klein, F., Baltensperger, U. and Prévôt, A. S. H.: Identification of significant precursor gases of secondary organic aerosols from residential wood combustion, 6, 27881, doi:10.1038/srep27881, 2016.

405 Canonica, S., Hellrung, B. and Wirz, J.: Oxidation of Phenols by Triplet Aromatic Ketones in Aqueous Solution, J. Phys. Chem. A, 104(6), 1226–1232, doi:10.1021/jp9930550, 2000.

Chang, J. L. and Thompson, J. E.: Characterization of colored products formed during irradiation of aqueous solutions containing H2O2 and phenolic compounds, Atmos. Environ., 44(4), 541–551, doi:https://doi.org/10.1016/j.atmosenv.2009.10.042, 2010.

410 Che, H., Segal-Rozenhaimer, M., Zhang, L., Dang, C., Zuidema, P., Dobracki, A., Sedlacek, A. J., Coe, H., Wu, H., Taylor, J., Zhang, X., Redemann, J. and Haywood, J.: Cloud processing and weeklong ageing affect biomass burning aerosol properties over the south-eastern Atlantic, Commun. Earth Environ., 3(1), 182, doi:10.1038/s43247-022-00517-3, 2022.

Chen, L.-W. A., Chow, J. C., Wang, X., Cao, J., Mao, J. and Watson, J. G.: Brownness of Organic Aerosol over the United States: Evidence for Seasonal Biomass Burning and Photobleaching Effects, Environ. Sci. Technol., 55(13), 8561–8572,
415 doi:10.1021/acs.est.0c08706, 2021.

Corral Arroyo, P., Bartels-Rausch, T., Alpert, P. A., Dumas, S., Perrier, S., George, C. and Ammann, M.: Particle-Phase Photosensitized Radical Production and Aerosol Aging, Environ. Sci. Technol., 52(14), 7680–7688, doi:10.1021/acs.est.8b00329, 2018.

Daumit, K. E., Carrasquillo, A. J., Sugrue, R. A. and Kroll, J. H.: Effects of Condensed-Phase Oxidants on Secondary Organic

420   Aerosol Formation, J. Phys. Chem. A, 120(9), 1386–1394, doi:10.1021/acs.jpca.5b06160, 2016.

Deng, J., Ma, H., Wang, X., Zhong, S., Zhang, Z., Zhu, J., Fan, Y., Hu, W., Wu, L., Li, X., Ren, L., Pavuluri, C. M., Pan, X., Sun, Y., Wang, Z., Kawamura, K. and Fu, P.: Measurement report: Optical properties and sources of water-soluble brown carbon in Tianjin, North China – insights from organic molecular compositions, Atmos. Chem. Phys., 22(10), 6449–6470, doi:10.5194/acp-22-6449-2022, 2022.

425   Ervens, B., Turpin, B. J. and Weber, R. J.: Secondary organic aerosol formation in cloud droplets and aqueous particles (aqSOA): a review of laboratory, field and model studies, Atmos. Chem. Phys., 11(21), 11069–11102, doi:10.5194/acp-11-11069-2011, 2011.

Farley, R., Bernays, N., Jaffe, D. A., Ketcherside, D., Hu, L., Zhou, S., Collier, S. and Zhang, Q.: Persistent Influence of Wildfire Emissions in the Western United States and Characteristics of Aged Biomass Burning Organic Aerosols under
430   Clean Air Conditions, Environ. Sci. Technol., 56(6), 3645–3657, doi:10.1021/acs.est.1c07301, 2022.

Garofalo, L. A., Pothier, M. A., Levin, E. J. T., Campos, T., Kreidenweis, S. M. and Farmer, D. K.: Emission and Evolution of Submicron Organic Aerosol in Smoke from Wildfires in the Western United States, ACS Earth Sp. Chem., 3(7), 1237–1247, doi:10.1021/acsearthspacechem.9b00125, 2019.

George, K. M., Ruthenburg, T. C., Smith, J., Yu, L., Zhang, Q., Anastasio, C. and Dillner, A. M.: FT-IR quantification of the
435   carbonyl functional group in aqueous-phase secondary organic aerosol from phenols, Atmos. Environ., 100, 230–237, doi:10.1016/j.atmosenv.2014.11.011, 2015.

Gilardoni, S., Massoli, P., Paglione, M., Giulianelli, L., Carbone, C., Rinaldi, M., Decesari, S., Sandrini, S., Costabile, F., Gobbi, G. P., Pietrogrande, M. C., Visentin, M., Scotto, F., Fuzzi, S. and Facchini, M. C.: Direct observation of aqueous secondary organic aerosol from biomass-burning emissions, Proc. Natl. Acad. Sci., 113(36), 10013–10018,
440   doi:10.1073/pnas.1602212113, 2016.

Heal, M. R., Harrison, M. A. J. and Neil Cape, J.: Aqueous-phase nitration of phenol by N2O5 and ClNO2, Atmos. Environ., 41(17), 3515–3520, doi:https://doi.org/10.1016/j.atmosenv.2007.02.003, 2007.

Herrmann, H., Hoffmann, D., Schaefer, T., Bräuer, P. and Tilgner, A.: Tropospheric Aqueous-Phase Free-Radical Chemistry: Radical Sources, Spectra, Reaction Kinetics and Prediction Tools, ChemPhysChem, 11(18), 3796–3822,
445   doi:https://doi.org/10.1002/cphc.201000533, 2010.

Herrmann, H., Schaefer, T., Tilgner, A., Styler, S. A., Weller, C., Teich, M. and Otto, T.: Tropospheric Aqueous-Phase Chemistry: Kinetics, Mechanisms, and Its Coupling to a Changing Gas Phase, Chem. Rev., 115(10), 4259–4334, doi:10.1021/cr500447k, 2015.

Hodzic, A., Kasibhatla, P. S., Jo, D. S., Cappa, C. D., Jimenez, J. L., Madronich, S. and Park, R. J.: Rethinking the global
450   secondary organic aerosol (SOA) budget: stronger production, faster removal, shorter lifetime, Atmos. Chem. Phys., 16(12), 7917–7941, doi:10.5194/acp-16-7917-2016, 2016.

Huang, D. D., Zhang, Q., Cheung, H. H. Y., Yu, L., Zhou, S., Anastasio, C., Smith, J. D. and Chan, C. K.: Formation and Evolution of aqSOA from Aqueous-Phase Reactions of Phenolic Carbonyls: Comparison between Ammonium Sulfate

and Ammonium Nitrate Solutions, Environ. Sci. Technol., doi:10.1021/acs.est.8b03441, 2018.

455   Jiang, H., Li, J., Sun, R., Tian, C., Tang, J., Jiang, B., Liao, Y., Chen, C.-E. and Zhang, G.: Molecular Dynamics and Light Absorption Properties of Atmospheric Dissolved Organic Matter, Environ. Sci. Technol., 55(15), 10268–10279, doi:10.1021/acs.est.1c01770, 2021a.

Jiang, W., Misovich, M. V, Hettiyadura, A. P. S., Laskin, A., McFall, A. S., Anastasio, C. and Zhang, Q.: Photosensitized Reactions of a Phenolic Carbonyl from Wood Combustion in the Aqueous Phase—Chemical Evolution and Light

460   Absorption Properties of AqSOA, Environ. Sci. Technol., 55(8), 5199–5211, doi:10.1021/acs.est.0c07581, 2021b.

Jiang, W., Ma, L., Niedek, C., Anastasio, C. and Zhang, Q.: Chemical and Light-Absorption Properties of Water-Soluble Organic Aerosols in Northern California and Photooxidant Production by Brown Carbon Components, In Preparation.

Jimenez, J. L., Canagaratna, M. R., Donahue, N. M., Prevot, A. S. H., Zhang, Q., Kroll, J. H., DeCarlo, P. F., Allan, J. D., Coe, H., Ng, N. L., Aiken, A. C., Docherty, K. S., Ulbrich, I. M., Grieshop, A. P., Robinson, A. L., Duplissy, J., Smith, J. D.,

465   Wilson, K. R., Lanz, V. A., Hueglin, C., Sun, Y. L., Tian, J., Laaksonen, A., Raatikainen, T., Rautiainen, J., Vaattovaara, P., Ehn, M., Kulmala, M., Tomlinson, J. M., Collins, D. R., Cubison, M. J., Dunlea, J., Huffman, J. A., Onasch, T. B., Alfarra, M. R., Williams, P. I., Bower, K., Kondo, Y., Schneider, J., Drewnick, F., Borrmann, S., Weimer, S., Demerjian, K., Salcedo, D., Cottrell, L., Griffin, R., Takami, A., Miyoshi, T., Hatakeyama, S., Shimono, A., Sun, J. Y., Zhang, Y. M., Dzepina, K., Kimmel, J. R., Sueper, D., Jayne, J. T., Herndon, S. C., Trimborn, A. M., Williams, L. R., Wood, E. C.,

470   Middlebrook, A. M., Kolb, C. E., Baltensperger, U. and Worsnop, D. R.: Evolution of Organic Aerosols in the Atmosphere, Science (80-.)., 326(5959), 1525–1529, doi:10.1126/science.1180353, 2009.

Kang, E., Toohey, D. W. and Brune, W. H.: Dependence of SOA oxidation on organic aerosol mass concentration and OH exposure: experimental PAM chamber studies, Atmos. Chem. Phys., 11(4), 1837–1852, doi:10.5194/acp-11-1837-2011, 2011.

475   Kaur, R. and Anastasio, C.: Light absorption and the photoformation of hydroxyl radical and singlet oxygen in fog waters, Atmos. Environ., 164, 387–397, doi:https://doi.org/10.1016/j.atmosenv.2017.06.006, 2017.

Kaur, R. and Anastasio, C.: First Measurements of Organic Triplet Excited States in Atmospheric Waters, Environ. Sci. Technol., 52(9), 5218–5226, doi:10.1021/acs.est.7b06699, 2018.

Kaur, R., Labins, J. R., Helbock, S. S., Jiang, W., Bein, K. J., Zhang, Q. and Anastasio, C.: Photooxidants from brown carbon

480   and other chromophores in illuminated particle extracts, Atmos. Chem. Phys., 19(9), 6579–6594, doi:10.5194/acp-19-6579-2019, 2019.

Kim, H., Collier, S., Ge, X., Xu, J., Sun, Y., Jiang, W., Wang, Y., Herckes, P. and Zhang, Q.: Chemical processing of water-soluble species and formation of secondary organic aerosol in fogs, Atmos. Environ., 200, 158–166, doi:https://doi.org/10.1016/j.atmosenv.2018.11.062, 2019.

485   Kleinman, L. I., Sedlacek III, A. J., Adachi, K., Buseck, P. R., Collier, S., Dubey, M. K., Hodshire, A. L., Lewis, E., Onasch, T. B., Pierce, J. R., Shilling, J., Springston, S. R., Wang, J., Zhang, Q., Zhou, S. and Yokelson, R. J.: Rapid evolution of aerosol particles and their optical properties downwind of wildfires in the western US, Atmos. Chem. Phys., 20(21),

13319–13341, doi:10.5194/acp-20-13319-2020, 2020.

Kobayashi, S. and Higashimura, H.: Oxidative polymerization of phenols revisited, Prog. Polym. Sci., 28(6), 1015–1048,
490   doi:10.1016/S0079-6700(03)00014-5, 2003.

Kroll, J. H., Smith, J. D., Che, D. L., Kessler, S. H., Worsnop, D. R. and Wilson, K. R.: Measurement of fragmentation and
functionalization pathways in the heterogeneous oxidation of oxidized organic aerosol, Phys. Chem. Chem. Phys., 11(36),
8005–8014, doi:10.1039/B905289E, 2009.

Kroll, J. H., Donahue, N. M., Jimenez, J. L., Kessler, S. H., Canagaratna, M. R., Wilson, K. R., Altieri, K. E., Mazzoleni, L.
495   R., Wozniak, A. S., Bluhm, H., Mysak, E. R., Smith, J. D., Kolb, C. E. and Worsnop, D. R.: Carbon oxidation state as a
metric for describing the chemistry of atmospheric organic aerosol, Nat Chem, 3(2), 133–139, doi:10.1038/nchem.948,
2011.

Kroll, J. H., Lim, C. Y., Kessler, S. H. and Wilson, K. R.: Heterogeneous Oxidation of Atmospheric Organic Aerosol: Kinetics
of Changes to the Amount and Oxidation State of Particle-Phase Organic Carbon, J. Phys. Chem. A, 119(44), 10767–
500   10783, doi:10.1021/acs.jpca.5b06946, 2015.

Lambe, A. T., Onasch, T. B., Croasdale, D. R., Wright, J. P., Martin, A. T., Franklin, J. P., Massoli, P., Kroll, J. H., Canagaratna,
M. R., Brune, W. H., Worsnop, D. R. and Davidovits, P.: Transitions from Functionalization to Fragmentation Reactions
of Laboratory Secondary Organic Aerosol (SOA) Generated from the OH Oxidation of Alkane Precursors, Environ. Sci.
Technol., 46(10), 5430–5437, doi:10.1021/es300274t, 2012.

505   Lambe, A. T., Cappa, C. D., Massoli, P., Onasch, T. B., Forestieri, S. D., Martin, A. T., Cummings, M. J., Croasdale, D. R.,
Brune, W. H., Worsnop, D. R. and Davidovits, P.: Relationship between Oxidation Level and Optical Properties of
Secondary Organic Aerosol, Environ. Sci. Technol., 47(12), 6349–6357, doi:10.1021/es401043j, 2013.

Lambe, A. T., Chhabra, P. S., Onasch, T. B., Brune, W. H., Hunter, J. F., Kroll, J. H., Cummings, M. J., Brogan, J. F., Parmar,
Y., Worsnop, D. R., Kolb, C. E. and Davidovits, P.: Effect of oxidant concentration, exposure time, and seed particles on
510   secondary organic aerosol chemical composition and yield, Atmos. Chem. Phys., 15(6), 3063–3075, doi:10.5194/acp-15-
3063-2015, 2015.

Lee, H. J. (Julie), Aiona, P. K., Laskin, A., Laskin, J. and Nizkorodov, S. A.: Effect of Solar Radiation on the Optical Properties
and Molecular Composition of Laboratory Proxies of Atmospheric Brown Carbon, Environ. Sci. Technol., 48(17), 10217–
10226, doi:10.1021/es502515r, 2014.

515   Leresche, F., Salazar, J. R., Pfotenhauer, D. J., Hannigan, M. P., Majestic, B. J. and Rosario-Ortiz, F. L.: Photochemical Aging
of Atmospheric Particulate Matter in the Aqueous Phase, Environ. Sci. Technol., doi:10.1021/acs.est.1c00978, 2021.

Li, M., Wang, X., Zhao, Y., Du, P., Li, H., Li, J., Shen, H., Liu, Z., Jiang, Y., Chen, J., Bi, Y., Zhao, Y., Xue, L., Wang, Y.,
Chen, J. and Wang, W.: Atmospheric Nitrated Phenolic Compounds in Particle, Gaseous, and Aqueous Phases During
Cloud Events at a Mountain Site in North China: Distribution Characteristics and Aqueous-Phase Formation, J. Geophys.
520   Res. Atmos., 127(18), e2022JD037130, doi:https://doi.org/10.1029/2022JD037130, 2022.

Liu, J., Lin, P., Laskin, A., Laskin, J., Kathmann, S. M., Wise, M., Caylor, R., Imholt, F., Selimovic, V. and Shilling, J. E.:

Optical properties and aging of light-absorbing secondary organic aerosol, Atmos. Chem. Phys., 16(19), 12815–12827, doi:10.5194/acp-16-12815-2016, 2016.

Ma, L., Guzman, C., Niedek, C., Tran, T., Zhang, Q. and Anastasio, C.: Kinetics and Mass Yields of Aqueous Secondary Organic Aerosol from Highly Substituted Phenols Reacting with a Triplet Excited State, Environ. Sci. Technol., 55(9), 5772–5781, doi:10.1021/acs.est.1c00575, 2021.

Mabato, B. R. G., Lyu, Y., Ji, Y., Li, Y. J., Huang, D. D., Li, X., Nah, T., Lam, C. H. and Chan, C. K.: Aqueous secondary organic aerosol formation from the direct photosensitized oxidation of vanillin in the absence and presence of ammonium nitrate, Atmos. Chem. Phys., 22(1), 273–293, doi:10.5194/acp-22-273-2022, 2022.

Misovich, M. V, Hettiyadura, A. P. S., Jiang, W., Zhang, Q. and Laskin, A.: Molecular-Level Study of the Photo-Oxidation of Aqueous-Phase Guaiacyl Acetone in the Presence of 3C*: Formation of Brown Carbon Products, ACS Earth Sp. Chem., 5(8), 1983–1996, doi:10.1021/acsearthspacechem.1c00103, 2021.

Morgan, W. T., Allan, J. D., Bower, K. N., Highwood, E. J., Liu, D., McMeeking, G. R., Northway, M. J., Williams, P. I., Krejci, R. and Coe, H.: Airborne measurements of the spatial distribution of aerosol chemical composition across Europe and evolution of the organic fraction, Atmos. Chem. Phys., 10(8), 4065–4083, doi:10.5194/acp-10-4065-2010, 2010.

Ng, N. L., Canagaratna, M. R., Zhang, Q., Jimenez, J. L., Tian, J., Ulbrich, I. M., Kroll, J. H., Docherty, K. S., Chhabra, P. S., Bahreini, R., Murphy, S. M., Seinfeld, J. H., Hildebrandt, L., Donahue, N. M., DeCarlo, P. F., Lanz, V. A., Prévôt, A. S. H., Dinar, E., Rudich, Y. and Worsnop, D. R.: Organic aerosol components observed in Northern Hemispheric datasets from Aerosol Mass Spectrometry, Atmos. Chem. Phys., 10(10), 4625–4641, doi:10.5194/acp-10-4625-2010, 2010.

Ng, N. L., Canagaratna, M. R., Jimenez, J. L., Chhabra, P. S., Seinfeld, J. H. and Worsnop, D. R.: Changes in organic aerosol composition with aging inferred from aerosol mass spectra, Atmos. Chem. Phys., 11(13), 6465–6474, doi:10.5194/acp-11-6465-2011, 2011.

O'Brien, R. E. and Kroll, J. H.: Photolytic Aging of Secondary Organic Aerosol: Evidence for a Substantial Photo-Recalcitrant Fraction, J. Phys. Chem. Lett., 10(14), 4003–4009, doi:10.1021/acs.jpclett.9b01417, 2019.

Olariu, R. I., Klotz, B., Barnes, I., Becker, K. H. and Mocanu, R.: FT–IR study of the ring-retaining products from the reaction of OH radicals with phenol, o-, m-, and p-cresol, Atmos. Environ., 36(22), 3685–3697, doi:https://doi.org/10.1016/S1352-2310(02)00202-9, 2002.

Palm, B. B., Peng, Q., Fredrickson, C. D., Lee, B. H., Garofalo, L. A., Pothier, M. A., Kreidenweis, S. M., Farmer, D. K., Pokhrel, R. P., Shen, Y., Murphy, S. M., Permar, W., Hu, L., Campos, T. L., Hall, S. R., Ullmann, K., Zhang, X., Flocke, F., Fischer, E. V and Thornton, J. A.: Quantification of organic aerosol and brown carbon evolution in fresh wildfire plumes, Proc. Natl. Acad. Sci., 117(47), 29469–29477, doi:10.1073/pnas.2012218117, 2020.

Pang, H., Zhang, Q., Lu, X., Li, K., Chen, H., Chen, J., Yang, X., Ma, Y., Ma, J. and Huang, C.: Nitrite-Mediated Photooxidation of Vanillin in the Atmospheric Aqueous Phase, Environ. Sci. Technol., 53(24), 14253–14263, doi:10.1021/acs.est.9b03649, 2019.

Saleh, R.: From Measurements to Models: Toward Accurate Representation of Brown Carbon in Climate Calculations, Curr.

Pollut. Reports, 6(2), 90–104, doi:10.1007/s40726-020-00139-3, 2020.

Schauer, J. J., Kleeman, M. J., Cass, G. R. and Simoneit, B. R. T.: Measurement of Emissions from Air Pollution Sources. 3. C1−C29 Organic Compounds from Fireplace Combustion of Wood, Environ. Sci. Technol., 35(9), 1716–1728, doi:10.1021/es001331e, 2001.

560 Sedlacek, A. J. I. I. I., Lewis, E. R., Onasch, T. B., Zuidema, P., Redemann, J., Jaffe, D. and Kleinman, L. I.: Using the Black Carbon Particle Mixing State to Characterize the Lifecycle of Biomass Burning Aerosols, Environ. Sci. Technol., 56(20), 14315–14325, doi:10.1021/acs.est.2c03851, 2022.

Shrivastava, M., Cappa, C. D., Fan, J., Goldstein, A. H., Guenther, A. B., Jimenez, J. L., Kuang, C., Laskin, A., Martin, S. T., Ng, N. L., Petaja, T., Pierce, J. R., Rasch, P. J., Roldin, P., Seinfeld, J. H., Shilling, J., Smith, J. N., Thornton, J. A.,

565 Volkamer, R., Wang, J., Worsnop, D. R., Zaveri, R. A., Zelenyuk, A. and Zhang, Q.: Recent advances in understanding secondary organic aerosol: Implications for global climate forcing, Rev. Geophys., 55(2), 509–559, doi:https://doi.org/10.1002/2016RG000540, 2017.

Smith, J. D., Sio, V., Yu, L., Zhang, Q. and Anastasio, C.: Secondary Organic Aerosol Production from Aqueous Reactions of Atmospheric Phenols with an Organic Triplet Excited State, Environ. Sci. Technol., 48(2), 1049–1057,

570 doi:10.1021/es4045715, 2014.

Smith, J. D., Kinney, H. and Anastasio, C.: Aqueous benzene-diols react with an organic triplet excited state and hydroxyl radical to form secondary organic aerosol, Phys. Chem. Chem. Phys., 17(15), 10227–10237, doi:10.1039/c4cp06095d, 2015.

Smith, J. D., Kinney, H. and Anastasio, C.: Phenolic carbonyls undergo rapid aqueous photodegradation to form low-volatility,

575 light-absorbing products, Atmos. Environ., 126, 36–44, doi:http://dx.doi.org/10.1016/j.atmosenv.2015.11.035, 2016.

Stefania, G., Paola, M., Marco, P., Lara, G., Claudio, C., Matteo, R., Stefano, D., Silvia, S., Francesca, C., Paolo, G. G., Chiara, P. M., Marco, V., Fabiana, S., Sandro, F. and Cristina, F. M.: Direct observation of aqueous secondary organic aerosol from biomass-burning emissions, Proc. Natl. Acad. Sci., 113(36), 10013–10018, doi:10.1073/pnas.1602212113, 2016.

Sun, Y., Zhang, Q., Zheng, M., Ding, X., Edgerton, E. S. and Wang, X.: Characterization and Source Apportionment of Water-

580 Soluble Organic Matter in Atmospheric Fine Particles (PM2.5) with High-Resolution Aerosol Mass Spectrometry and GC–MS, Environ. Sci. Technol., 45(11), 4854–4861, doi:10.1021/es200162h, 2011.

Sun, Y. L., Zhang, Q., Anastasio, C. and Sun, J.: Insights into secondary organic aerosol formed via aqueous-phase reactions of phenolic compounds based on high resolution mass spectrometry, Atmos. Chem. Phys., 10(10), 4809–4822, doi:10.5194/acp-10-4809-2010, 2010.

585 Ulbrich, I. M., Canagaratna, M. R., Zhang, Q., Worsnop, D. R. and Jimenez, J. L.: Interpretation of organic components from Positive Matrix Factorization of aerosol mass spectrometric data, Atmos. Chem. Phys., 9(9), 2891–2918, doi:10.5194/acp-9-2891-2009, 2009.

Wagstrom, K. M. and Pandis, S. N.: Determination of the age distribution of primary and secondary aerosol species using a chemical transport model, J. Geophys. Res. Atmos., 114(D14), doi:https://doi.org/10.1029/2009JD011784, 2009.

590 Yang, J., Au, W. C., Law, H., Lam, C. H. and Nah, T.: Formation and evolution of brown carbon during aqueous-phase nitrate-mediated photooxidation of guaiacol and 5-nitroguaiacol, Atmos. Environ., 254, 118401, doi:https://doi.org/10.1016/j.atmosenv.2021.118401, 2021.

Yee, L. D., Kautzman, K. E., Loza, C. L., Schilling, K. A., Coggon, M. M., Chhabra, P. S., Chan, M. N., Chan, A. W. H., Hersey, S. P., Crounse, J. D., Wennberg, P. O., Flagan, R. C. and Seinfeld, J. H.: Secondary organic aerosol formation

595 from biomass burning intermediates: phenol and methoxyphenols, Atmos. Chem. Phys., 13(16), 8019–8043, doi:10.5194/acp-13-8019-2013, 2013.

Yu, L., Smith, J., Laskin, A., Anastasio, C., Laskin, J. and Zhang, Q.: Chemical characterization of SOA formed from aqueous-phase reactions of phenols with the triplet excited state of carbonyl and hydroxyl radical, Atmos. Chem. Phys., 14(24), 13801–13816, doi:10.5194/acp-14-13801-2014, 2014.

600 Yu, L., Smith, J., Laskin, A., George, K. M., Anastasio, C., Laskin, J., Dillner, A. M. and Zhang, Q.: Molecular transformations of phenolic SOA during photochemical aging in the aqueous phase: competition among oligomerization, functionalization, and fragmentation, Atmos. Chem. Phys., 16(7), 4511–4527, doi:10.5194/acp-16-4511-2016, 2016.

Zhai, L., An, Y., Feng, L., Qin, X. and Xu, J.: Contrasting the physical and chemical characteristics of dissolved organic matter between glacier and glacial runoff from a mountain glacier on the Tibetan Plateau, Sci. Total Environ., 848, 157784,

605 doi:https://doi.org/10.1016/j.scitotenv.2022.157784, 2022.

Zhang, Q., Jimenez, J. L., Canagaratna, M. R., Ulbrich, I. M., Ng, N. L., Worsnop, D. R. and Sun, Y.: Understanding atmospheric organic aerosols via factor analysis of aerosol mass spectrometry: a review, Anal. Bioanal. Chem., 401(10), 3045–3067, doi:10.1007/s00216-011-5355-y, 2011.

Zhou, S., Collier, S., Jaffe, D. A., Briggs, N. L., Hee, J., Sedlacek III, A. J., Kleinman, L., Onasch, T. B. and Zhang, Q.:

610 Regional influence of wildfires on aerosol chemistry in the western US and insights into atmospheric aging of biomass burning organic aerosol, Atmos. Chem. Phys., 17(3), 2477–2493, doi:10.5194/acp-17-2477-2017, 2017.

Zhou, S., Collier, S., Jaffe, D. A. and Zhang, Q.: Free tropospheric aerosols at the Mt. Bachelor Observatory: more oxidized and higher sulfate content compared to boundary layer aerosols, Atmos. Chem. Phys., 19(3), 1571–1585, doi:10.5194/acp-19-1571-2019, 2019.

615